Processing and Application of Ceramics 13 [3] (2019) 300–309
https://doi.org/10.2298/PAC1903300K

Microstructure-property relations of biphasic calcium phosphate obtained by hot pressing process

Krai Kulpetchdara[1,2], Apichart Limpichaipanit[1], Chamnan Randorn[3], Gobwute Rujijanagul[1], Tawee Tunkasiri[1], Komsanti Chokethawai[1,4,*]

[1]*Department of Physics and Materials Science, Faculty of Science, Chiang Mai University, Chiang Mai 50200, Thailand*
[2]*PhD's Degree Program in Materials Science, Faculty of Science, Chiang Mai University, Chiang Mai 50200, Thailand*
[3]*Department of Chemistry, Faculty of Science, Chiang Mai University, Chiang Mai 50200, Thailand*
[4]*Center of Excellence in Materials Science and Technology, Chiang Mai University, Chiang Mai 50200, Thailand*

Received 19 December 2018; Received in revised form 20 May 2019; Accepted 19 August 2019

Abstract

Biphasic calcium phosphate (BCP) was fabricated through hot pressing process from hydroxyapatite (HA) starting powder synthesized by a peroxide-based precipitation method and dried at 250 °C. The synthesized HA powder contained some calcium hydrogen phosphate (CHP) as a minor phase. In this work, the dense BCP ceramics with a mixture of HA and β-TCP phases were successfully obtained by hot pressing at temperature ranging from 700–1100 °C. The amount of HA phase in the hot pressed samples decreased with increasing sintering temperature from 700 to 900 °C, while the amount of β-TCP exhibited an opposite trend. The relations between the microstructure and mechanical properties of the dense BCP ceramics sintered in the temperature range 700–1100 °C were investigated. The sample hot pressed at 800 °C has a dense structure with the highest hardness (4.86 ± 0.19 GPa) and the lowest fracture toughness (0.80 ± 0.01 MPa·m$^{1/2}$). In addition, biocompatibility of apatite layer formed after immersion in simulated body fluid (SBF) for 14 days can be observed by SEM images. The results revealed that the samples hot-pressed at 800 and 900 °C were covered by calcium phosphate (CaP) crystal layer indicating the strong interaction of BCP ceramics and SBF.

Keywords: *hydroxyapatite powder, hot pressing, biphasic calcium phosphate, biomineralization*

I. Introduction

Biphasic calcium phosphate (BCP) is generally composed of non-resorbable hydroxyapatite (HA) and resorbable tricalcium phosphate (β-TCP) [1] or mixture of α-TCP and β-TCP [2]. BCP ceramics show great potential for bone tissue engineering applications because of their excellent biocompatibility, bioactivity and osteoconductivity [3]. Ordinal scale in extent of reabsorption of calcium phosphate (CaP) in different phases is: amorphous calcium phosphate (ACP) > α-TCP > β-TCP > HA [4]. The thermal decomposition of HA to β-TCP occurs at sintering temperatures as low as 850 °C. During sintering at 1120 °C, the β-TCP is the stable phase [5]. Furthermore, the phase transformation of α-TCP is expected upon heating from sintering temperatures higher than 1120 °C. The solubility and biodegradation rate of α-TCP are much higher than those of β-TCP [6]. Thermal stability and phase transformations of HA to β-TCP and β-TCP to ℵ-TCP as well as the phase transition temperatures depend on stoichiometry and synthesis method of hydroxyapatite [7]. The Ca^{2+} and PO_4^{3-} ions of the β-TCP would be helpful in accelerating the new bone formation. HA is non-resorbable and it exhibits slow osteoconduction *in vivo* [8]. The extent of reabsorption of BCP depends on the β-TCP/HA ratio; the higher the ratio, the higher the extent of reabsorption [9]. BCP with the β-TCP/HA ratio of 0.667 can

*Corresponding author: tel: +6653 943 367,
e-mail: *komsanti.chokethawai@cmu.ac.th*

reabsorb more than 50%, which is equivalent to bone ingrowth after 1–2 years of implantation [10].

Nanostructured ceramics can be fabricated by compacting nanopowders at high temperatures and pressures where sintering time and atmosphere can be varied. Pressure assisted methods, such as hot pressing, are also applied to obtain nanostructured HA ceramics [11]. Hot pressing processes can decrease the temperature of the onset of densification and suppress the grain growth, resulting in higher final density. This leads to fine microstructures, higher thermal stability and subsequently better mechanical properties of calcium orthophosphate [12]. This technique is generally used to process HA ceramics with a controlled microstructure.

Recently, many researchers have synthesized the biphasic calcium phosphate by various techniques, such as a mechanical blending of the desired amounts of HA and β-TCP, hydrothermal method, vacuum-assisted foaming as well as several other approaches [12–14]. In this work, the investigation of BCP synthesized by hot pressing process with the HA powder prepared using a peroxide-based route (PBR) was conducted [13–15]. Biomineralization of apatite layer after immersion in simulated body fluid (SBF) was observed. The relationship between microstructure and properties was also discussed.

II. Material and methods

2.1. Hydroxyapatite powder synthesis

The hydroxyapatite powders were synthesized using a peroxide based route as reported in our previous papers [13,14]. In brief, the HA powders were synthesized using calcium nitrate tetrahydrate ($Ca(NO_3)_2 \cdot 4\,H_2O$, Sigma Aldrich), hydrogen peroxide (Merck), ortho-phosphoric acid (RCL Labscan) and ammonium hydroxide (J.T. Baker) as starting chemicals. $Ca(NO_3)_2 \cdot 4\,H_2O$ was dissolved in 5% v/v H_2O_2 and H_3PO_4 was then slowly added dropwise into the solution in stoichiometric amount with continuous stirring. The pH of the solution was adjusted to pH = 9 by NH_4OH solution and the mixture was stirred continuously for 30 min at ambient temperature. The white calcium phosphate compounds were filtered and washed with distilled water for several times. The synthesized HA powders were dried at 250 °C for 12 h and dry ball milled using the equal amount of balls with diameters of 10, 15 and 20 mm. The ratio of the milling media to HA powder was 3 : 1 by volume and the milling time was 15 min.

2.2. Biphasic calcium phosphate fabrication

The prepared HA powder was placed into a graphite mould (diameter of 12 mm) and hot-pressed at various temperatures, i.e. 700, 800, 900 and 1100 °C (to obtain samples with notation HA700, HA800, HA900 and HA1100, respectively) for 2 h under a pressure of 25 MPa in air. Hot-press system consisted of heating and pressing parts. The heating system of the furnace consisted of a heating coil and a hydraulic press was used to apply uniaxial pressure. The temperature control system was installed to ensure that the correct temperature was obtained. The heating rate was 10 °C/min and the samples were cooled naturally in the hot-press chamber.

2.3. Characterization

The density, water absorption and porosity were measured by the Archimedes' method, using distilled water as the immersion media.

The hardness of the sintered samples was measured by Vickers indentation by first preparing a high quality, smoothly polished surface with no pre-cracking. The polished specimens were then indented by a Vickers pyramidal microhardness indenter. The Vickers hardness of the sample at top surface was determined (STARTECH SMV-1000) using load of 0.98 N applied for 10 s and 10 measurements were performed for each sample.

Fracture toughness was calculated by indentation using the equation:

$$K_{IC} = 0.016\left(\frac{E}{HV}\right)^{1/2}\frac{P}{C^{3/2}} \qquad (1)$$

where P is the load, C is the crack length from the centre of the indent to the crack tip, E is the Young's modulus (80 GPa for HA) and HV is the Vickers hardness.

The synthesized powders and sintered samples were analysed by XRD using a Rigaku Mini Flex II X-ray diffractometer with a Cu K wavelength of 1.5418 Å. Measuring was carried out from 20 to 50° (2θ) with 0.01°/step. The peaks obtained for all samples were compared to standard reference JCPDS files.

The simulated body fluid (SBF), a solution with an ionic concentration close to human blood plasma, was prepared following to the Kokubo's protocol [16]. The dense HA ceramics were immersed in SBF for 14 days at 36.5 °C and pH = 7.4 (adjusted with tris(hydroxymethylaminomethane) and hydrochloric acid). After immersion, the dense HA ceramics were rinsed with distilled water and dried in air. Free-surface and cross section of samples were observed by SEM.

SEM microscope (JEOL JSM-IT300LV) was used to characterize the morphology of the powder, HA ceramics and samples after SBF soaking and energy-dispersive spectroscopy (EDS Oxford Instruments INCAx-sight Elemental Detector) to determine elemental composition. The HA powder samples were loaded directly into the SEM holder using graphite tape and were covered with gold in a sputtering device. To prepare the cross-section samples, the HA ceramics were first cut and then mounted on resin before polishing. The sintered samples were ground with SiC sand paper, and then polished with a diamond suspension and afterwards gold coated. The ratio of calcium to phosphorus (Ca/P) in the coatings was measured using an energy dispersive spectroscopy.

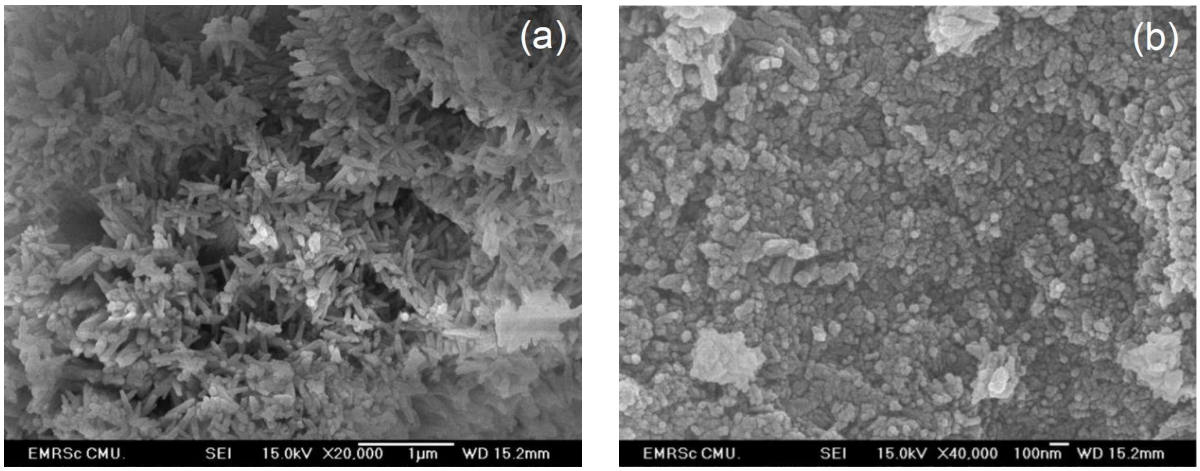

Figure 1. SEM image of the HA powder: a) before and b) after milling

Thermogravimetric analyses were useful to determine the weight loss during the thermal treatment at high temperature. TGA/DSC system (TGA/DSC1 Metter Toledo Beaumont Leys, UK) was used to determine the reference temperature (T_r) and the sample temperature (T_s) by heating the dried HA powders from room temperature to 1200 °C at a heating rate of 10 °C/min in alumina crucibles.

III. Results and discussion

The morphology of the HA powder synthesized by chemical precipitation method is represented in Fig. 1. Figure 1a shows the morphology of the synthesized HA powder before milling. It can be seen that the un-milled HA powder has needle-like particles with particle size of ~50 nm (width) × 100 nm (length). The reduction of the particle size compared to the conventional chemical route was due to the fact that the hydrogen peroxide acts as a chelating agent, leading to a growth inhibition [13]. After milling, the HA powder has nanoscale structure (~50 nm) but no characteristic needle-like morphology, as shown in Fig. 1b. The amounts of Ca and P in the HA powders, determined by EDS, are 23.84 and 12.71 at.%, respectively giving a Ca/P molar ratio of 1.88.

XRD pattern of the HA powder is shown in Fig. 2.

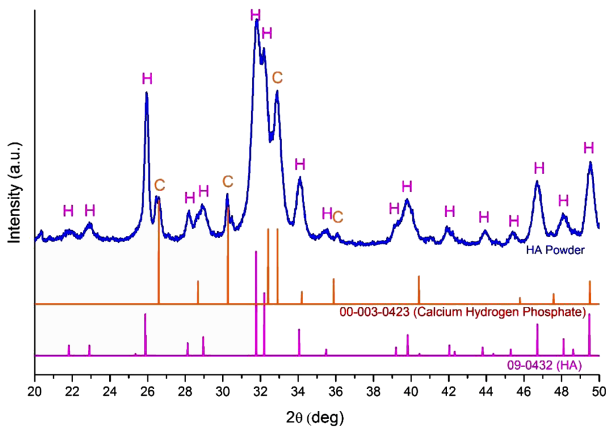

Figure 2. XRD pattern of the HA powder

It corresponded to that of pure hydroxyapatite (HA) phase, $Ca_{10}(PO_4)_6(OH)_2$ (JCPDS 09-0432), as the main phase and a trace of the second phase corresponded to calcium hydrogen phosphate (CHP) (JCPDS 003-0423). This is in agreement with the EDS results which revealed the high Ca/P molar ratio (1.88) of the powder sample. The Ca/P of the pure HA is 1.67, hence this higher Ca/P ratio implied the presence of another component, which is calcium hydrogen phosphate (CHP). The presence of CHP as a minor phase was confirmed by XRD data (Fig. 2). It has been reported that CHP can be generated during the drying process with temperature lower than transition point (400 °C) [7].

Amounts of crystalline phases (HA and calcium hydrogen phosphate) in the powder was determined by the reference intensity ratio (RIR) technique [18–20]. Volume fraction of HA can be determined by the following formula:

$$HA = \frac{I_{HA}}{I_{HA} + I_{CHP}} \tag{2}$$

where I_{HA} and I_{CHP} refer to the relative intensity of the most intense peak of HA and CHP phases, respectively. According to the XRD results presented in Fig. 2, the volume fractions of HA and CHP in the powder, calculated by Eq. 2, are about 89.4% and 10.6%, respectively.

Thermal analysis (TGA/DSC) was carried out to investigate the thermal stability of the synthesized HA powder. After heating the HA powder in chamber from 30 to 1200 °C, the result revealed that three peaks on the TGA/DSC graph, determining endothermic and exothermic reactions, can be seen (Fig. 3). These correspond to the degradation of organic material occurring between 270 and 280 °C (in agreement with Moussa *et al.* [21]) and decarbonation between 440 and 490 °C (reported by Park *et al.* [22]). This decarbonation process is related to the carbon decomposition [23]. These carbonate ions were formed as a result of CO_2 being absorbed by the calcium phosphate [22,24]. The HA was dehydroxylated and transformed to oxyhydroxyapatite (OHA) at 760–810 °C [9] by completely reversible reaction in accordance with the following equation [25]:

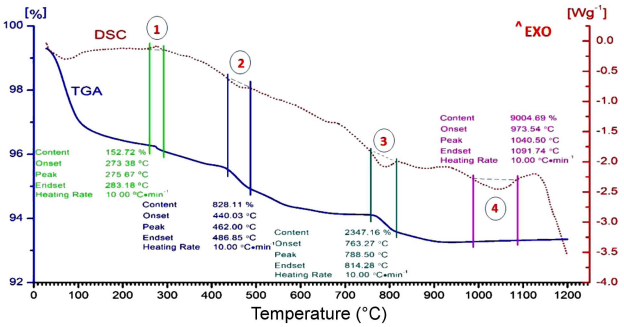

Figure 3. TGA/DSC result of the HA powder: [1] the degradation of organic material, [2] decarbonation, [3] HA dehydroxylated and transformed to oxyhydroxyapatite, and [4] phase transition of HA to β-TCP

$$Ca_{10}(PO_4)_6(OH)_2 \rightarrow Ca_{10}(PO_4)_6(OH)_{2-2x}O_x + xH_2O_{(g)}$$

The decomposition of HA to β-TCP occurs from 970 to 1090 °C [26]. The dehydroxylation of HA would partially form dehydroxylated (OHA) or completely dehydroxylated oxyhydroxyapatite (OA) and phase transition of HA to β-TCP and TTCP can occur, which can be written as [25]:

$$Ca_{10}(PO_4)_6(OH)_2 \rightarrow {}_2Ca_3(PO_4)_2 + Ca_4P_2O_9 + H_2O_{(g)}$$

In general, temperature required for the pure HA phase formation is approximately 400–700 °C [14,27–31]. In the present work, the dried HA powders at temperature of 250 °C was chosen as a starting material for hot pressing, which is slightly lower than that reported. This may be useful in terms of energy saving, less time consuming and lower production cost to fabricate the HA powder.

Figure 4 presents the results of the XRD analysis of the HA samples obtained by hot pressing. Considering the XRD pattern of the HA1100 sample, it can be seen that HA (JCPDS 09-0432), β-TCP (JCPDS 09-0169) and α-TCP (JCPDS 09-0348) are present. Some XRD peaks of β-TCP can also be seen in the sintered samples (e.g. 1010 at 2θ of 25.8°, 0210 at 2θ of 31.02°, 132 at 2θ of 24.09° and 043 at 2θ of 34.18°). On the other hand, the peaks of HA became narrower after sintering (e.g. 210 at 2θ of 28.96° and 202 at 2θ of 34.05°) which means that HA had a larger grain size.

The volume faction of HA can be determined via the following formula:

$$HA = \frac{I_{HA}}{I_{HA} + I_{\beta-TCP} + I_{\alpha-TCP}} \quad (3)$$

where I_{HA}, $I_{\beta-TCP}$ and $I_{\alpha-TCP}$ refer to the relative intensity of the most intense peaks of HA, β-TCP and α-TCP phases, respectively [20]. According to the results presented in Fig. 4, the volume fractions of HA, β-TCP and α-TCP were calculated by Eq. 3 and shown in Table 1. The amount of HA phase decreases with increasing sintering temperature while the amount of β-TCP has an opposite trend. Furthermore, the XRD patterns of the HA700, HA800 and HA900 show that β-TCP is still maintained as the major phase, and HA is the minor phase. This result is attributed to the fact that the HA powder contains CHP as a minor phase [31]. Moreover, the XRD pattern of the sintered HA1100 sample (Fig. 4) reveals α-TCP as the major phase with β-TCP as secondary phase and HA is the minor phase. Some researchers have reported that decomposition into third phase proceeded above 1200 °C [32,33] while some reported decomposition occurred when sintered at 1150 °C [34].

Table 1. The volume percentage of the HA, β-TCP and α-TCP in the ceramics

Sample	HA [%]	β-TCP [%]	α-TCP [%]
HA700	18.95	81.05	0
HA800	16.51	83.49	0
HA900	15.42	84.58	0
HA1100	18.81	33.76	47.43

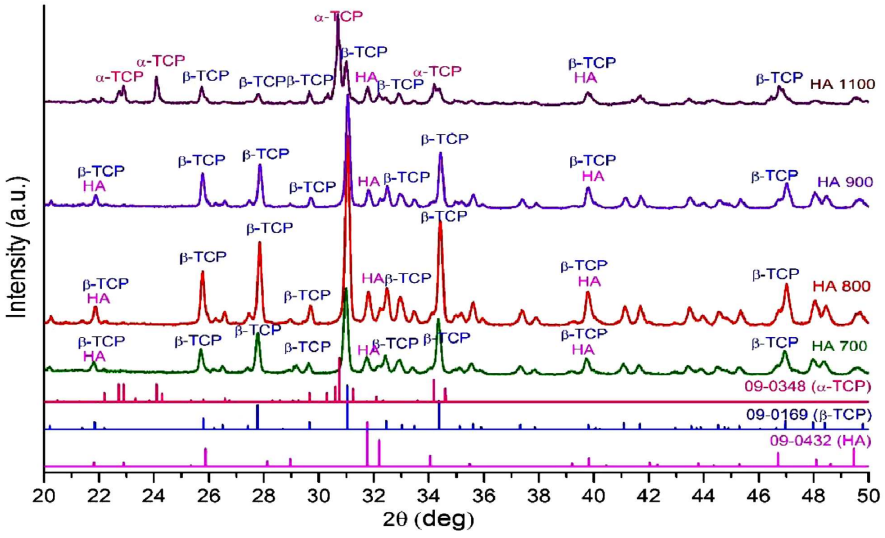

Figure 4. XRD patterns of the HA samples at various sintering temperature

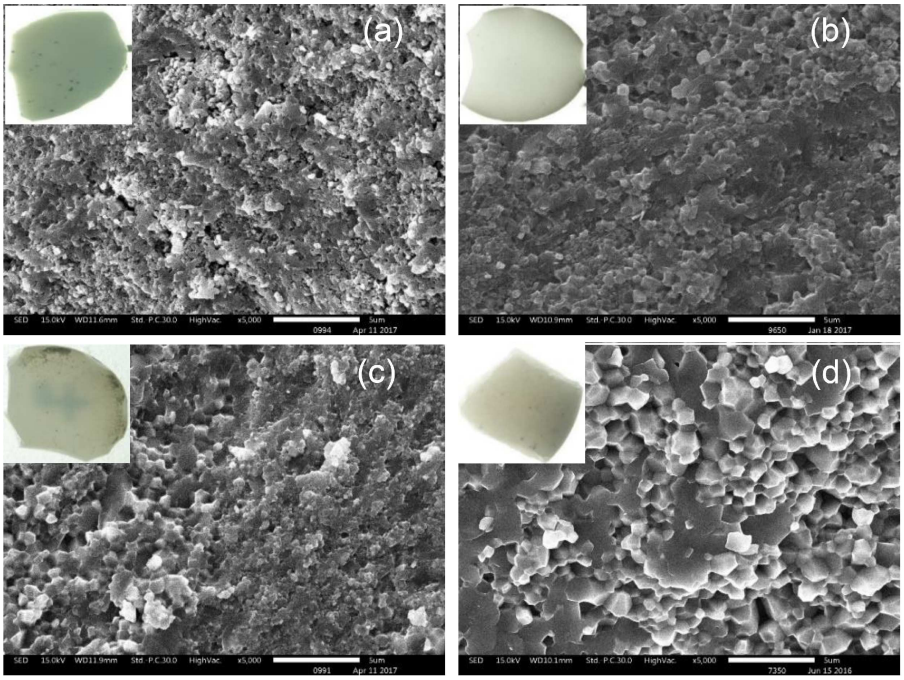

Figure 5. SEM micrographs of fracture surface of (a) HA700, (b) HA800, (c) HA900 and (d) HA1100

As shown in Fig. 3 and confirmed by XRD results presented in Fig. 4, BCP formation starts at above 700 °C. Normally, HA decomposes to β-TCP phase at 950 °C, and β-TCP decomposes to α-TCP at 1150 °C [2]. Hot pressing technique provides an additional driving force (pressure) to promote densification and prevents grain growth by decreasing sintering temperature and time [35].

The effect of hot pressing temperature on the microstructure of the HA samples is observed in SEM images shown in Fig. 5. When the HA powder was hot pressed at temperatures higher than 800 °C, dense HA ceramics with smaller grain size can be obtained. The grain size of the sintered HA1100 sample (approximately 1 μm, Fig. 5d) is bigger than the other samples (which have grain sizes of 200–500 nm, Figs. 5a-c). On the other hand, the sample HA900 exhibited a bimodal grain size distribution with the presence of some individual large grains, ranging between 500 and 900 nm as shown in Fig. 5c. The sintered samples HA800, HA900 and HA1100 were translucent, as can be seen in insets of Fig. 5. They reached nearly full density because high translucency requires pore-free microstructure [11,12,36]. All the samples exhibited increasing grain size trend with increasing sintering temperature. The crystallinity of the HA and β-TCP depends on the sintering temperature: the higher the sintering temperature, the higher the crystallinity [35].

In general, hot pressing technique is helpful for suppressing grain boundary migration and reducing grain boundary diffusion rate, resulting in high densification of BCP [18]. The physical properties of the HA samples are shown in Table 2. The values of apparent porosity (*AP*) and bulk density (*BD*) of the samples HA800 and HA900 were consistent with SEM results. The physical properties of the HA samples affected the microhardness. The Vickers hardness (*HV*) values of the HA800, HA900 and HA1100 are higher than that for the sample HA700 because of higher density. The *AP* and *HV* values of the HA700 (Table 2) confirm that the sample is still not fully sintered. This phenomenon is due to the fact that the ions do not obtain sufficient energy at 700 °C for their rearrangement in the lattice and complete crystallization of HA. These results show that 700 °C as sintering temperature is not high enough to provide the driving force for full densification. Below that critical temperature the grain boundary diffusion, as the dominant mechanism for the sintering of nanopowders in the final sintering stage, seems to be exhausted, so that the full density cannot be obtained. From data presented in Table 2, it is obvious that a decrease in *AP* results in an increase in *HV* with temperature increase to 800 °C. The reduction of densification in the HA ceramics causes slower grain growth and an average grain

Table 2. The values of apparent porosity and bulk density of the HA samples

	HA700	HA800	HA900	HA1100
Apparent porosity, *AP* [%]	6.42	0.08	0.11	0.32
Water absorption, *WA* [%]	2.2766	0.0257	0.0347	0.1104
Bulk density, *BD* [g/cm^3]	2.82	3.08	3.07	2.93
Vickers hardness, *HV* [GPa]	3.02 ± 0.39	4.86 ± 0.19	4.77 ± 0.22	4.75 ± 0.22
Fracture toughness [MPa·m$^{1/2}$]	1.25 ± 0.04	0.80 ± 0.01	0.97 ± 0.05	1.16 ± 0.11

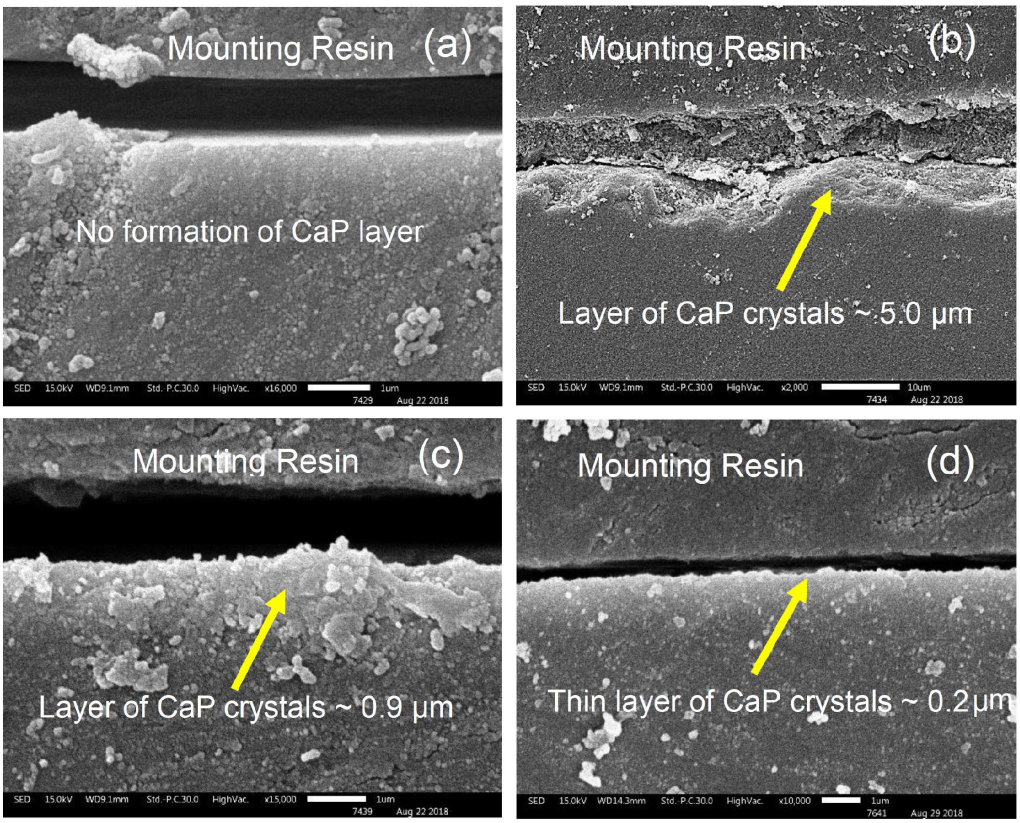

Figure 6. SEM images of cross section surface of the ceramics after soaking in SBF for 7 days (a) HA700, (b) HA800, (c) HA900 and (d) HA1100

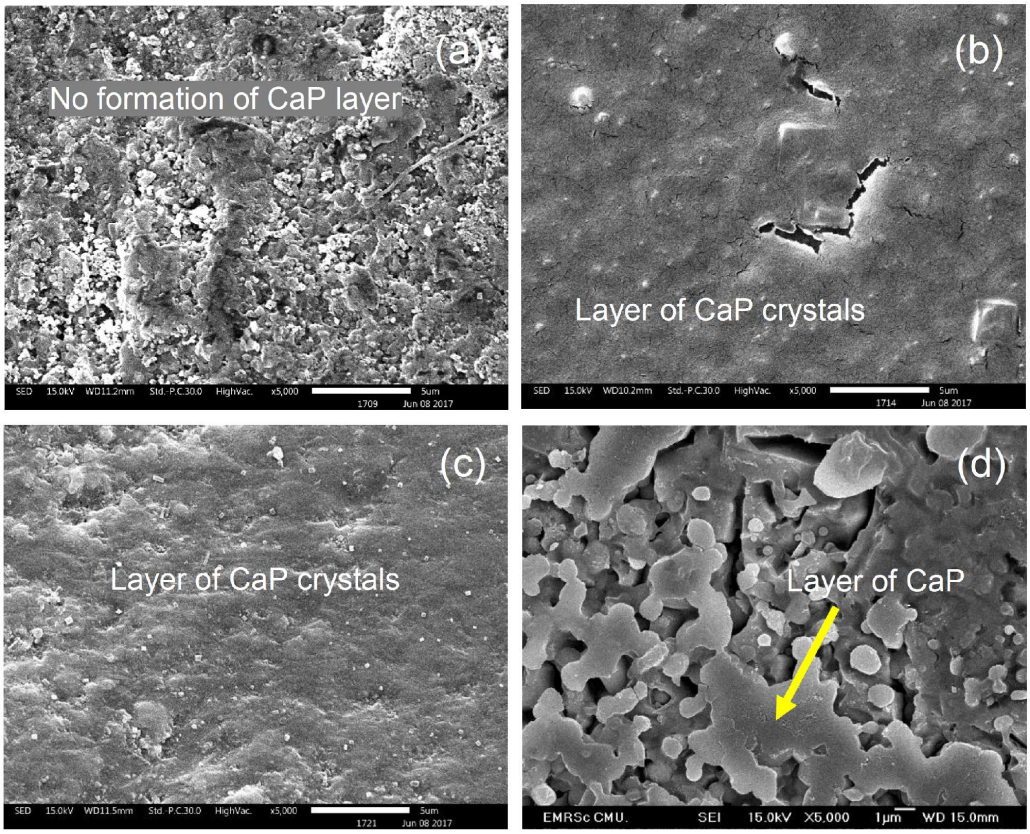

Figure 7. SEM images of fracture surface of the ceramics after soaking in SBF: a) HA700, b) HA800, c) HA900 and d) HA1100

size over 0.4 μm is obtained [37]. The mean *HV* value of the HA800 (4.86 ± 0.19 GPa) is considerably higher than for the conventionally sintered samples (1.98 GPa) at lower temperature [38].

Figure 6 shows the SEM images of cross sections of the HA samples after soaking in SBF for 7 days. It can be clearly seen that no formation of calcium phosphate (CaP) layer was observed on the surface of the HA700 (Fig. 6a) whereas the HA800 and HA900 (Figs. 6b and 6c) were covered with a higher amount of CaP crystals. The layer thicknesses of the samples HA800 and HA900 are ~5 μm and ~0.9 μm, respectively. However, the HA1100 sample was covered only with a thin layer of CaP crystals (~0.2 μm) as shown in Fig. 6d. The composition of HA/TCP corresponding to 20/80 occurred at the fastest rate *in vivo* over the other formulations of the more stable 100% HA, and the fully degradable, 100% TCP [1,8].

Figure 7 shows SEM images of fracture surface of the samples after soaking in SBF for 14 days. Faceted fracture surface in the HA700 sample (Fig. 7a) without any layer was observed. However, the HA800 and HA900 samples (Figs. 7b and 7c) were covered with a higher amount of CaP crystals. This indicated that the BCP ceramics interacted strongly with the SBF. The reabsorption behaviour was highly dependent on the β-TCP/HA ratio, the higher β-TCP/HA ratio, the greater reabsorption and surface properties appear to exert the greatest influence on reabsorption [38]. Figure 7d shows a thin CaP layer partially covering on the surface because the reabsorption was less pronounced (lower β-TCP/HA ratio).

Comparison of the properties of HA ceramics obtained in this work with those obtained by various sintering techniques is shown in Table 3. It should be noted that *HV* value (*HV* ~ 4.86 GPa) for the HA800 pro-

Table 3. Average grain size *D*, Vickers hardness *HV*, bulk density *BD*, relative density *RD* and fracture toughness K_{IC} of the fabricated hot pressed HA ceramics compared with other literature data

Sintering conditions	Preparation (supplier)	Characteristics/properties					Ref.
		Composition Ca/P ratio	*D* [μm]	*HV* [GPa]	*BD* [g·cm^{-3}] (*RD* [%])	K_{IC} [MPa·m$^{1/2}$]	
HP 1250 °C/30 min, argon, 20 MPa, 15 °C/min	Commercial powder (Bioland, France)	HA 1.67	0.4	-	(99.5)	1.2	[39]
HP 1100 °C/30 min, argon, 20 MPa, 20 °C/min	Wet precipitation^{LM}, filtration	98HA/2β-TCP 1.663	0.6 ± 0.2	-	(99.9)	1.0 ± 0.1	[37]
HP 950 °C/1 h, argon, 20 MPa	Wet precipitation^{LM}, Spray-drying	HA 1.67	0.38	4.3	1.89 (60)	1.52	[11]
HP 1000 °C/1 h, vacuum, 40 MPa	Commercial HA and hexagonal BN	HA/BN/TCP	0.7	6.5	(99)	-	[40]
HP 1320 °C/1 h, nitrogen, 20 MPa	Wet precipitation^{LM}, filtration	HA/Al_2O_3/some glass phases	-	5.5 ± 1.9	-	2.80 ± 0.10	[41]
Pressureless sintering, 1150 °C/2 h, air, 2 °C/min	Wet precipitation^{LM}, filtration	HA 1.67	-	7.24	(99)	1.22	[42]
Pressureless sintering, 1300 °C/2 h, air, 2 °C/min	Wet precipitation^{LM}, filtration	HA 1.67	~2.0	4.3	(98)	0.9	[43]
Conventional sintering, 1400 °C/2 h, air, 2 °C/min	Wet precipitation^{LM}, filtration	HA *N/A*	2–5	-	(99)	0.6 ± 0.01	[44]
HIP sintering, 1100 °C/1 h, 160 MPa Ar/O_2, 5 °C/min	Wet precipitation^{LM}, filtration	80HA/20β-TCP	0.73	5.7	(98)	0.92	[45]
Two step sintering, 1100/1050 °C/20 h, 5 °C/min	Wet precipitation^{LM}, filtration	HA/β-TCP	0.375	4.9 ± 0.09	3.07 ± 0.02 (97.27)	1.11 ± 0.04	[46]
Conventional sintering 1400 °C/2 h, air, 5 °C/min	Commercial HA powders, TiO_2 and Al_2O_3 nanopowders	HA/TCP HA/Al_2O_3 HA/R&A-TiO_2		2.52 4.21 5.12	(89) (90) (93)		[47]
Conventional sintering, 1400 °C/2 h, air, 5 °C/min	Cockle shells Egg shells	75HA/25β-TCP	14.15	5.5	3.02 (96)		[48]
Conventional sintering, 1200 °C/2 h, air, 5 °C/min	Wet precipitation^{LM}, filtration	HA/TCP	0.9	5.67	3.10 (98.22)		[14]
HP 1200 °C/30 min, argon, 25 MPa	Bovine bone	HA	~2	4.9 ± 0.2	3.08 ± 0.02	0.5 ± 0.1	[49]
HP 800 °C/2 h, air, 25 MPa	Wet precipitation^{LM}, filtration	20HA/80β-TCP 1.39	0.5	4.86 ± 0.19	3.08 (97.59)	*N/A*	This work

N/A - data not available; CIP - cold isostatic pressing; ^{LM} - laboratory made

Table 4. EDS result of the HA ceramic samples

Element	HA700	HA700 SBF	HA800	HA800 SBF	HA900	HA900 SBF	HA1100 SBF
O K	60.68	63.96	54.96	65.31	67.23	65.42	47.75
P K	16.57	15.23	18.85	14.72	14.27	14.83	20.22
Ca K	22.75	20.81	26.19	19.97	18.49	19.75	32.04
Ca/P	1.37	1.37	1.39	1.36	1.30	1.33	1.58

duced by hot press technique in the present work was slightly higher than that reported in the literature and fabricated under similar conditions (by hot pressing at sintering temperature of 800–950 °C and pressure of 20 MPa). The results in this work show significantly lower sintering temperature compared to the other researches where the sintered ceramics had the similar hardness [14,46,48,49].

The EDS results in Table 4 show that the Ca/P ratio range of HA sample is 1.3–1.58. The samples prepared by hot pressing with Ca/P < 1.667 yielded bi-phasic mixtures of HA-TCP. On the other hand, the amount of TCP in the two phase mixtures increased as a function of decreasing Ca/P ratio [50,51]. After SBF soaking, that ratio did not change, which means the observed covering layer is the BCP layer [51,52].

IV. Conclusions

The dense biphasic calcium phosphate (BCP) ceramics with a mixture of HA and β-TCP phases were successfully obtained by hot pressing at temperatures higher than 700 °C. In general, the HA phase transforms to β-TCP at the temperature of about 850 °C and the transformation of β-TCP to α-TCP occurs at temperatures greater than 1125 °C. However, in this hot pressing process, the sintering temperature of BCP ceramics can be kept under 800 °C while obtaining dense ceramics. The relations between the development of microstructure and the hardness of the dense BCP ceramics sintered in the temperature range 700–1100 °C can be clearly seen in this research. The maximum hardness of dense HA ceramics reached 4.86 GPa which is higher than that of BCP ceramics produced previously by the hot pressing process under the same sintering conditions. In addition, after immersion in simulated body fluid (SBF) apatite layer was formed on the surfaces of the samples hot-pressed at 800 and 900 °C confirming strong interaction of BCP ceramics and SBF.

Acknowledgement: The authors would like to thank the Graduate School, Chiang Mai University. This research was funded by the National Research Council of Thailand (NRCT) grant no. ΠUV/2557-26 and Center of Excellence in Materials Science and Technology, Chiang Mai University.

References

1. R.W.N. Nilen, P.W. Richter, "The thermal stability of hydroxyapatite in biphasic calcium phosphate ceramics", *J. Mater. Sci. Mater. Med.*, **19** (2008) 1693–1702.
2. S.V. Dorozhkin, "Biphasic, triphasic and multiphasic calcium orthophosphates", *Acta Biomater.*, **8** (2012) 963–977.
3. Q. Wu, X. Zhang, B. Wu, W. Huang, "Fabrication and characterization of porous HA/β-TCP scaffolds strengthened with micro-ribs structure", *Mater. Lett.*, **92** (2013) 274–277.
4. G. Daculsi, "Biphasic calcium phosphate concept applied to artificial bone, implant coating and injectable bone substitute", *Biomaterials*, **19** (1998) 1473–1478.
5. R. Vani, E.K. Girija, K. Elayaraja, S.P. Parthiban, R. Kesavamoorthy, S.N. Kalkura, "Hydrothermal synthesis of porous triphasic hydroxyapatite/(α and β) tricalcium phosphate", *J. Mater. Sci. Mater. Med.*, **20** (2009) 43–48.
6. Y. Li, W. Weng, K.C. Tam, "Novel highly biodegradable biphasic tricalcium phosphates composed of α-tricalcium phosphate and β-tricalcium phosphate", *Acta Biomater.*, **3** (2007) 251–254.
7. S. Raynaud, E. Champion, D. Bernache-Assollant, P. Thomas, "Calcium phosphate apatites with variable Ca/P atomic ratio. I. Synthesis, characterisation and thermal stability of powders", *Biomaterials*, **23** (2002) 1065–1072.
8. A. Macchetta, I.G. Turner, C.R. Bowen, "Fabrication of HA/TCP scaffolds with a graded and porous structure using a camphene-based freeze-casting method", *Acta Biomater.*, **5** (2009) 1319–1327.
9. T.L. Arinzeh, T. Tran, J. Mcalary, G. Daculsi, "A comparative study of biphasic calcium phosphate ceramics for human mesenchymal stem-cell-induced bone formation", *Biomaterials*, **26** (2005) 3631–3638.
10. T.J. Levingstone, *Ceramics for Medical Applications*, Dublin City University, Ireland, 2008.
11. Dj. Veljović, B. Jokić, R. Petrović, E. Palcevskis, A. Dindune, I.N. Mihailescu, Dj. Janaćković, "Processing of dense nanostructured HAP ceramics by sintering and hot pressing", *Ceram. Int.*, **35** (2009) 1407–1413.
12. S.V. Dorozhkin, "Calcium orthophosphate-based bioceramics", *Materials*, **6** (2013) 3840–3942.
13. K. Kulpetchdara, A. Limpichaipanit, G. Rujijanagul, C. Randorn, K. Chokethawai, "Influence of the nano hydroxyapatite powder on thermally sprayed HA coatings onto stainless steel", *Surf. Coat. Technol.*, **306** [part A] (2016) 181–186.
14. C. Randorn, A. Kanta, K. Yaemsunthorn, G. Rujijanagul, "Fabrication of dense biocompatible hydroxyapatite ceramics with high hardness using a peroxide-based route: a potential process for scaling up", *Ceram. Int.*, **41** (2015) 5594–5599.
15. A. Han, G. Rujijanagul, C. Randorn, "Preparation of hydroxyapatite hydrogel for bone-like materials via novel self-initiated photocatalytic polymerization", *Mater. Lett.*, **193** (2017) 142–145.
16. T. Kokubo, H. Takadama, "How useful is SBF in predicting in vivo bone bioactivity", *Biomaterials*, **27** (2006) 2907–2915.
17. K. Ozeki, H. Aoki, Y. Fukui, "Effect of pH on crystalliza-

tion of sputtered hydroxyapatite film under hydrothermal conditions at low temperature", *J. Mater. Sci.*, **40** (2005) 2837–2842.
18. E. Lifshin, *X-Ray Characterization of Materials*, Wiley-VCH, New York, 1999.
19. F.H. Chung, "Quantitative interpretation of X-ray diffraction patterns of mixtures. I. Matrix-flushing method of quantitative multi component analysis", *J. Appl. Cryst.*, **7** (1974) 519–525.
20. R.C. Garvie, P.S. Nicholson, "Phase analysis in zirconia systems", *J. Am. Ceram. Soc.*, **55** [6] (1972) 303–305.
21. S.B. Moussa, H. Bachouâ, M. Gruselle, P. Beaunier, A. Flambard, B. Badraoui, "Hybrid organic-inorganic materials based on hydroxyapatite structure", *J. Solid State Chem.*, **248** (2017) 171–177.
22. E. Park, Sr. R.A. Condrate, D. Lee, K. Kociba, P.K. Gallagher, "Characterization of hydroxyapatite: Before and after plasma spraying", *J. Mater. Sci. Mater. Med.*, **13** (2002) 211–218.
23. A. Tampieri, G. Celotti, S. Sprio, C. Mingazzini, "Characteristics of synthetic hydroxyapatites and attempts to improve their thermal stability", *Mater. Chem. Phys.*, **64** (2000) 54–61.
24. F. Granados-Correa, J. Bonifacio-Martínez J. Serrano-Gómez, "Synthesis and characterization of calcium phosphate and its relation to Cr(VI) adsorption properties", *Rev. Int. Contam. Ambient.*, **26** [2] (2010) 129–134.
25. N. Monmaturapoj, C. Yatongchai, "Effect of sintering on microstructure and properties of hydroxyapatite produced by different synthesizing methods", *J. Met. Mater. Min.*, **20** [2] (2010) 53–61.
26. T.M. Sridhar, U.K. Mudali, M. Subbaiyan, "Sintering atmosphere and temperature effects on hydroxyapatite coated type 316L stainless steel", *Corros. Sci.*, **45** [10] (2003) 2337–2359.
27. S. Laasri, M. Taha, A. Laghzizil, E.K. Hlil, J. Chevalier, "The affect of densification and dehydroxylation on the mechanical properties of stoichiometric hydroxyapatite bioceramics", *Mater. Res. Bull.*, **45** (2010) 1433–1437.
28. L.H. He, O.C. Standard, T.T.Y. Huang, B.A. Latella, M.S. Swain, "Mechanical behavior of porous hydroxyapatite", *Acta Biomater.*, **4** (2008) 577–586.
29. K.A. Gross, L.M. Rodriguez-Lorenzo, "Sintered hydroxyfluorapatites. Part I: sintering ability of precipitated solid solution powders", *Biomaterials*, **25** (2004) 1375–1384.
30. S. Ramesh, C.Y. Tan, S.B. Bhaduri, W.D. Teng, I. Sopyan, "Densification behavior of nanocrystalline hydroxyapatite bioceramics", *J. Mater. Process. Technol.*, **206** (2008) 221–230.
31. M. Mazaheri, M. Haghighatzadeh, A.M. Zahedi, S.K. Sadrnezhaad, "Effect of a novel sintering process on mechanical properties of hydroxyapatite ceramics", *J. Alloys Compd.*, **471** (2009) 180–184.
32. I.M. Hung, W.J. Shin, M.H. Hon, M.C. Wang, "The properties of sintered calcium phosphate with [Ca]/[P] = 1.5", *Int. J. Mol. Sci.*, **13** (2012) 13569–13586.
33. M. Ebrahimi, M.G. Botelho, S.V. Dorozhkin, "Biphasic calcium phosphates bioceramics (HA/TCP): Concept, physicochemical properties and the impact of standardization of study protocols in biomaterials research", *Mater. Sci. Eng. C*, **71** (2017) 1293–1312.
34. A. Tampieri, G. Celotti, F. Szontagh, E. Landi, "Sintering and characterization of HA and TCP bioceramics with control of their strength and phase purity", *J. Mater. Sci. Mater. Med.*, **8** (1997) 29–37.
35. E. Champion, "Sintering of calcium phosphate bioceramics", *Acta Biomater.*, **9** (2013) 5855–5875.
36. J.E. Barralet, G.J.P. Fleming, C. Campion, J.J. Harris A.J. Wright, "Formation of translucent hydroxyapatite ceramics by sintering in carbon dioxide atmospheres", *J. Mater. Sci.*, **38** (2003) 3979–3993.
37. S. Raynaud, E. Champion, J.P. Lafon, D. Bernache-Assollant, "Calcium phosphate apatites with variable Ca/P atomic ratio III. Mechanical properties and degradation in solution of hot pressed ceramics", *Biomaterials*, **23** (2002) 1081–1089.
38. Gunawan, I. Sopyan, S. Nurfaezah, M. Ammar, "Development of triphasic calcium phosphate-carbon nanotubes (HA/TCP-CNT) composite: A preliminary study", *Key Eng. Mater.*, **531-532** (2012) 258–261.
39. R. Halouani, D. Bernache-Assolant, E. Champion, A. Ababou, "Microstructure and related mechanical properties of hot pressed hydroxyapatite ceramics", *J. Mater. Sci. Mater. Med.*, **5** (1994) 563–568.
40. P. Ekavianty, H. Young-Hwan, K. Byung Nam, K. Young-Moon, L. Kyeongseok, J. Young-Keun, K. Doo-In, K. Kwang-Ho, K. Sukyoung, "Characterization of boron nitride-reinforced hydroxyapatite composites prepared by spark plasma sintering and hot press", *J. Ceram. Soc. Jpn.*, **121** [4] (2013), 344–347.
41. Z. Xihua, L. Changxia, L. Musen, B. Yunqiang, and S. Junlong, "Fabrication of hydroxyapatite/diopside/alumina composites by hot-press sintering process", *Ceram. Int.*, **35** (2009) 1969–1973.
42. S. Ramesh, C.Y. Tan, R. Tolouei, M. Amiriyan, J. Purbolaksono, I. Sopyan, W.D. Teng, "Sintering behavior of hydroxyapatite prepared from different routes", *Mater. Des.*, **34** (2012) 148–154.
43. S. Ramesh, K.L. Aw, R. Tolouei, M. Amiriyan, C.Y. Tan, M. Hamdi, J. Purbolaksono, M.A. Hassan, W.D. Teng, "Sintering properties of hydroxyapatite powders prepared using different methods", *Ceram. Int.*, **39** (2013) 111–119.
44. S. Nath, K. Biswas, K. Wang, R.K. Bordia, B. Basu, "Sintering, phase stability, and properties of calcium phosphate-mullite composites", *J. Am. Ceram. Soc.*, **93** [6] (2010) 1639–1649.
45. M. Descamps, L. Boilet, G Moreau, A. Tricoteaux, J. Lu, A. Leriche, V. Lardot, F. Cambier, "Processing and properties of biphasic calcium phosphates bioceramics obtained by pressureless sintering and hot isostatic pressing", *J. Eur. Ceram. Soc.*, **33** (2013) 1263–1270.
46. M. Lukić, Z. Stojanović, S.D. Škapin, M. Maček-Kržmanc, M. Mitrić , S. Marković, D. Uskoković, "Dense fine-grained biphasic calcium phosphate (BCP) bioceramics designed by two-step sintering", *J. Eur. Ceram. Soc.*, **31** (2011) 19–27.
47. M. Aminzare, A. Eskandari, M.H. Baroonian, A. Berenov, Z. Razavi Hesabi, M. Taheri, S.K. Sadrnezhaad, "Hydroxyapatite nanocomposites: Synthesis, sintering and mechanical properties", *Ceram. Int.*, **39** (2013) 2197–2206.
48. N. Lertcumfu, P. Jaita, S. Manotham, P. Jarupoom, S. Eitssayeam, K. Pengpat, G. Rujijanagul, "Properties of calcium phosphates ceramic composites derived from natural materials", *Ceram. Int.*, **42** (2016) 10638–10644.
49. J. Brzezińska-Miecznik, K. Haberko, M.M. Bućko, G.

Grabowski, M. Sitarz, "Hydroxyapatite of natural origin - zirconia composites, preparation and reactions within the system", *Process. Appl. Ceram.*, **10** [4] (2016) 219–225.
50. A. Cüneyt Tas, "Combustion synthesis of calcium phosphate bioceramic powders", *J. Eur. Ceram. Soc.*, **20** (2000) 2389–2394.
51. M. Ebrahimian-Hosseinabadi, M. Etemadifar, F. Ashrafizadeh, "Effects of nano-biphasic calcium phosphate composite on bioactivity and osteoblast cell behavior in tissue engineering applications", *J. Med. Signals Sens.*, **6** [4] (2016) 237–242.
52. S. Jalota, S.B. Bhaduri, A. Cüneyt Tas, "In vitro testing of calcium phosphate (HA, TCP, and biphasic HA-TCP) whiskers", *J. Biomed. Mater. Res. A*, **78A** [3] 481–490.